Acta Pharmaceutica Sinica B 2021;11(4):1021−1029

Chinese Pharmaceutical Association
Institute of Materia Medica, Chinese Academy of Medical Sciences

Acta Pharmaceutica Sinica B

www.elsevier.com/locate/apsb
www.sciencedirect.com

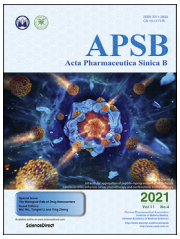

ORIGINAL ARTICLE

Intracellular uptake of nanocrystals: Probing with aggregation-induced emission of fluorescence and kinetic modeling

Jifen Zhang[a,b], **Clairissa D. Corpstein**[b], **Tonglei Li**[b,*]

[a]*College of Pharmaceutical Sciences, Southwest University, Chongqing 400716, China*
[b]*Department of Industrial and Physical Pharmacy, Purdue University, West Lafayette, IN 47907, USA*

Received 28 July 2020; received in revised form 19 September 2020; accepted 21 September 2020

KEY WORDS

Nanocrystal;
Intracellular uptake;
Aggregation-induced emission;
Pharmacokinetics;
Tetrakis(4-hydroxyphenyl) ethylene;
Fate;
Dissolution kinetics;
Absorption mechanism

Abstract Nanocrystal formulations have been explored to deliver poorly water-soluble drug molecules. Despite various studies of nanocrystal formulation and delivery, much more understanding needs to be gained into absorption mechanisms and kinetics of drug nanocrystals at various levels, ranging from cells to tissues and to the whole body. In this study, nanocrystals of tetrakis (4-hydroxyphenyl) ethylene (THPE) with an aggregation-induced emission (AIE) property was used as a model to explore intracellular absorption mechanism and dissolution kinetics of nanocrystals. Cellular uptake studies were conducted with KB cells and characterized by confocal microscopy, flow cytometry, and quantitative analyses. The results suggested that THPE nanocrystals could be taken up by KB cells directly, as well as in the form of dissolved molecules. The cellular uptake was found to be concentration- and time-dependent. In addition, the intracellular THPE also could be exocytosed from cells in forms of dissolved molecules and nanocrystals. Kinetic modeling was conducted to further understand the cellular mechanism of THPE nanocrystals based on first-order ordinary differential equations (ODEs). By fitting the kinetic model against experimental measurements, it was found that the initial nanocrystal concentration had a great influence on the dynamic process of dissolution, cellular uptake, and exocytosis of THPE nanocrystals. As the nanocrystal concentration increased in the culture media, dissolution of endocytosed nanocrystals became enhanced, subsequently driving the efflux of THPE molecules from cells.

*Corresponding author.
E-mail address: tonglei@purdue.edu (Tonglei Li).

Peer review under responsibility of Chinese Pharmaceutical Association and Institute of Materia Medica, Chinese Academy of Medical Sciences.

https://doi.org/10.1016/j.apsb.2020.09.017

1. Introduction

Drug nanocrystals are crystalline drug particles typically regarded with a diameter smaller than 1 μm. Nanocrystals have been widely used to improve oral bioavailability of poorly water-soluble drugs because of their enhanced dissolution rates and the likelihood of adhesion to intestine membranes due to their small size[1−3]. Nanocrystal production generally requires straightforward formulation steps and becomes amenable for scale-up production[4,5]. Nanocrystal-based products are also suitable for many administration routes due to their versatility in different dosage forms (such as oral tablets and parenteral suspensions)[6−8]. Nanocrystals have become one of the most actively researched drug delivery systems, especially for delivering poorly soluble drugs[9−11].

Development of nanocrystals has been greatly explored over recent decades, with a focus on preparation optimization, stabilizer screening, structure characterization, and solubility and dissolution enhancement, as well as improvement of *in vivo* bioavailability[12−15]. However, little is known about how nanocrystals interact with cells and cellular components, their transmembrane absorption mechanisms and kinetics, and, more importantly, their *in vivo* fate including dissolution kinetics and biological distribution. The lapse in knowledge stems from the current lack of reliable analytical approaches to truthfully discern and quantify nanocrystals *vs.* molecules in a biological milieu[16]. The total amount of nanocrystals plus dissolved drug molecules is generally analyzed and quantified. As such, the current lack in understanding of *in vivo* behaviors, mechanisms, and biological performance of drug nanocrystals limits advances towards greater commercial success.

Fortunately, some efforts have been made to explore the *in vivo* fate of nanocrystals[17,18]. Strategies include observing crystalline morphology in slices with transmission electron microscopy (TEM)[19], and tracking nanocrystals with autofluorescence or physically embedded fluorophores[20−24]. The last method presents a promising idea for nanocrystal quantification. Fluorescent probes that optically quench in water or have aggregation-induced emission (AIE) properties have been used to discriminate between nanocarriers and free drugs[25−27]. Therefore, these kinds of probes are effective to explore the *in vivo* fate of nanocrystals.

In one of our previous studies of drug nanocrystals, paclitaxel nanocrystals (PTX-NCs) integrated with tetraphenylethylene (TPE), an AIE probe[28,29], were used to investigate cellular uptake mechanisms[30,31]. TPE has four aromatic rings conjugated together *via* rigid ethylene (Fig. 1). When integrated into PTX-NCs, its molecular motion is restricted and the excited state dissipation occurs optically *via* photon emission, generating fluorescence. When released from PTX-NCs and dissolved in bulk medium, its aromatic groups are free to rotate, losing its fluorescence characteristics[32−34]. Because of the AIE property, understanding of how PTX-NCs were transported across cell membranes, as well as the intracellular dissolution kinetics, was achieved. Nonetheless, some limitations remained when using TPE as an AIE probe to study drug nanocrystals. The solubility of TPE is marginal (about 0.032 μg/mL measured in this study), making it highly possible to recrystallize once it is released from hybrid TPE drug nanocrystals. Measured fluorescence may have also resulted from TPE-NCs, as well as from PTX/TPE-NCs.

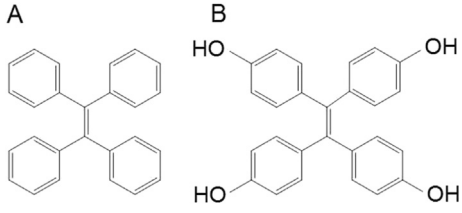

Figure 1 Structures of tetraphenylethylene (TPE, A) and tetrakis (4-hydroxyphenyl) ethylene (THPE, B).

To address possible uncertainties of characterizing nanocrystals because of the poor solubility of TPE, tetrakis (4-hydroxyphenyl) ethylene (THPE) was used as an AIE probe in this study. THPE is a derivative of TPE with one hydrogen atom replaced by hydroxyl group in each phenyl ring (Fig. 1), giving a much higher water solubility (about 2.6 μg/mL as measured in this study), about 80 times than that of TPE. In addition, instead of forming hybrid nanocrystals with another drug, pure THPE nanocrystals (THPE-NCs) were prepared and used in cellular studies. Because of its inherent AIE property, THPE-NCs permitted us to thoroughly explore cellular uptake mechanisms and kinetics, further our conclusion from the previous study. Kinetic modeling was established to interpret transmembrane kinetics of THPE-NC suspensions measured at different concentrations.

2. Experimental methodology

2.1. Materials

THPE of ≥97% purity was purchased from TCI (Portland, OR, USA). Gibco® folate free RPMI-1640 medium and fetal bovine serum (FBS) were purchased from Life Technologies (Grand Island, NY, USA).

2.2. Preparation and characterization of THPE-NCs

THPE-NCs were prepared by anti-solvent precipitation. Briefly, 2.0 mg of THPE was dissolved in 1 mL of ethanol and then quickly added to 40 mL of deionized water at 4 °C under stirring (800 rpm) and sonication in an ice-water bath (FS20D Bath Sonicator by Thermofisher Inc., Waltham, MA, USA). The mixture was stirred and sonicated for 10 min. Upon crystallization, the suspension was filtered through a 50 nm polycarbonate filter. The precipitation was re-suspended in 3 mL deionized water by sonication in an ice-water bath.

Particle size and zeta potential of THPE-NCs were measured by a dynamic light scattering instrument (Zetasizer 3000HS by Malvern Inc., Worcestershire, UK) at room temperature. The morphology of THPE-NCs was detected by a scanning electron microscope (SEM, Nova Nano SEM by FEI Co., Hillsboro, OR, USA). THPE-NCs on a 50-nm polycarbonate filter were dried at room temperature and sputter-coated with gold and palladium for 60 s before imaging.

The AIE property of THPE-NCs was characterized by suspending THPE-NCs in a series of mixtures of ethanol and water at various *v/v* ratios. Fluorescence of the samples was measured using a FluoroMax-2 Spectrofluorimeter (Horiba Ltd., Piscataway, NJ, USA) with an excitation at 350 nm and an emission at 450 nm. The samples were centrifuged at 15,000 rpm for 15 min (Sorvall MX 150 plus centrifuge by Thermofisher Inc., Waltham, MA, USA) to separate dissolved THPE molecules and THPE-NCs. The

content of THPE in the supernatant and pellets were analyzed by HPLC.

THPE concentration analysis was carried out using an Agilent 1200 HPLC system (Agilent, Santa Clara, CA, USA) with an RP-18 column (150 mm × 4.6 mm with pore size of 5 μm; Agilent Co., Philadelphia, PA, USA). The mobile phase consisted of acetonitrile and water (46: 54, *v*/*v*). The flow rate was 1.0 mL/min and the detection wavelength was 330 nm. The quantitative lower limit of THPE in this study was 0.0146 μg/mL.

2.3. Cell culture

KB cells (nasopharyngeal epidermal carcinoma) were obtained from American Type Culture Collection (ATCC, Manassas, VA, USA) and used between passages 18−24. The cells were cultured in RPMI-1640 medium supplemented with 10% (*v*/*v*) FBS and 1% penicillin streptomycin at 37 °C in a saturated humidity of 5% CO_2. KB cells were seeded at a density of 2×10^5 cells/well and were cultured for 24 h before incubation with THPE-NCs.

2.4. Cellular uptake of THPE-NCs

Cellular uptake of THPE-NCs was quantified using confocal microscopy, flow cytometry, and HPLC. KB cells were prepared as stated above. THPE-NC suspension was diluted with cell medium sans FBS to a total THPE concentration of 24, 8, or 2.7 μg/mL, respectively.

For confocal microscopy, KB cells were seeded in confocal petri dishes. After cell adhesion to dish walls, THPE-NC suspension of 2.7 or 24 μg/mL was incubated with cells for 1, 3, or 7 h. Additionally, cells incubated for 3 h were washed with PBS and incubated in 1 mL of fresh medium for an additional 1, 2, or 5 h (4, 5, or 8 h total) to determine. At the end of each time point, cells were then gently washed with cold PBS three times and stained with 8 μmol/L DiI for 30 min at 37 °C. Cells were immediately imaged by laser scanning confocal microscopy (Nikon Ai, Nikon Co., Tokyo, Japan).

Cell uptake observed by flow cytometry was carried out as described in our previous studies[31]. KB cells were seeded in 6-well plates (Corning, NY, USA). After 24 h, medium in each well was discarded, and 1 mL of THPE-NCs was added and incubated with cells for 0.5, 1, 2, and 3 h. For those incubated for 3 h, cells were washed with PBS and incubated in 1 mL of fresh medium for an additional 1 or 2 h (4 or 5 h total). At all pre-determined times, cells were washed three times with cold PBS, detached with trypsin, resuspended in PBS, and measured using flow cytometry (BD Co., San Jose, CA, USA) within 2 h. A blank control was obtained using the same procedure, with 1 mL of fresh medium.

Cellular uptake was quantified by HPLC as described in our previous study[28]. Cells were treated by the same procedure as used in the preparation for flow cytometry. Extracellular media were immediately centrifuged at 15,000 rpm for 15 min (Thermofisher Inc.) to separate THPE-NCs from dissolved molecules. Once the THPE supernatant was removed, THPC-NCs were dissolved in 1 mL of methanol. Respective concentrations of THPE in the supernatant and dissolved THPE-NCs were determined by HPLC. In addition, 1 mL of cell suspensions was lysed by sonication (Selecta Solupuls, Nickon A1, Nikon Co., Tokyo, Japan) in an ice bath and further dissolved in 1 mL of methanol. The total amount of THPE was measured by HPLC.

2.5. PK modeling and simulation of NC cellular uptake

To understand the mechanism and kinetics of cellular uptake of nanocrystals, transport of THPE uptake and removal from cells was modeled with first-order kinetic models. Fig. 2 shows the kinetic pathways taken by extra- and intra-cellular THPE nanocrystals and molecules. Transmembrane transport is assumed to be in equilibrium between respective nanocrystals and molecules. Only dissolution of the nanocrystals is considered, due to the fact that THPE suspensions were used to incubate with cells.

The ordinary differential equation (ODE) model was solved by *ode 45* in Matlab version 2019.b2 (MathWorks Co., Natick, MA, USA) and the rate parameters were determined by *lsqcurvefit* in Matlab by fitting ODE-predicted concentration values against experimental data determined by HPLC. The parameters values were then used in simulation drug concentrations under other incubation conditions.

2.6. Statistical analyses of data

All data were expressed as mean ± standard deviation (SD). One-way ANOVA was used to test the differences between groups and $P < 0.05$ or $P < 0.01$ was considered to be a significant difference.

3. Results and discussion

3.1. Nanocrystal characterization

The size of THPE-NCs was found to be 313.5 ± 23.0 nm with a PDI of 0.240 ± 0.029 ($n = 3$). The zeta potential of THPE-NCs was −18.2 ± 1.9 mV. An SEM micrograph (Fig. 3) showed THPE-NCs had a prism-like morphology approximately 300 nm in length.

To confirm the larger solubility of THPE in relation to TPE, and to test THPE's AIE property, dissolution studies of THPE nanocrystals in various ratios of ethanol:water were carried out. As shown in Fig. 4, THPE-NC fluorescence decreased as ethanol content increased from 0 to 16%, showing gradual dissolution of THPE-NCs. At 18% EtOH, almost no fluorescence was detected, indicating complete THPE-NCs dissolution. By contrast, complete TPE dissolution only occurred

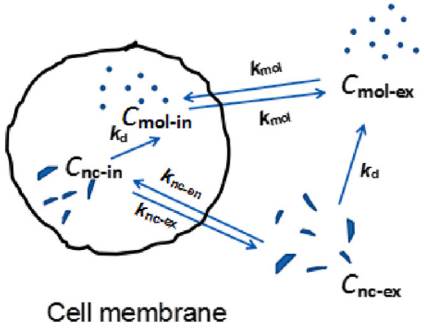

Figure 2 Schematic depicting transportation of THPE across cell membrane, including both molecules and nanocrystals. *C* denotes concentration and *k* rate constant, with subscripts nc and mol representing nanocrystal and molecule, and en, ex, in, and d representing endocytosis, exocytosis, intracellular and dissolution.

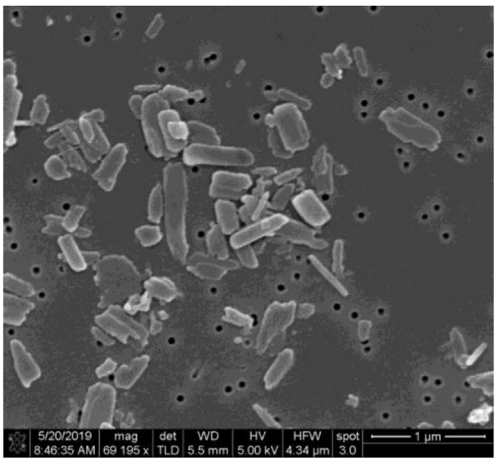

Figure 3 SEM image of tetrakis (4-hydroxyphenyl) ethylene nanocrystals THPE-NCs.

when the content of ethanol was equal to or over 70%[31], suggesting that THPE had a better aqueous solubility than TPE. Positive correlations were observed between fluorescence and undissolved THPE-NCs, approximated by two linear regions between 0 and 7.22 μg/mL ($r = 0.9953$) and between 7.22 and 26.16 μg/mL ($r = 0.9982$). Depending on the measured fluorescence, a suitable linear region was selected to calculate the nanocrystal concentration of a sample. These tests further validated the AIE property of THPE-NCs.

3.2. *Cellular uptake studies*

3.2.1. *Cellular uptake determined by confocal microscopy imaging*

Confocal microscopy was a useful tool to observe the drug uptake by cells directly. In this study, uptake of THPE-NCs by KB cells was observed qualitatively by confocal laser scanning microscopy (CLSM, Fig. 5). Since THPE had good AIE property, only undissolved THPE, *i.e.* THPE-NCs, could emit fluorescence. Therefore, the observed fluorescence within cells verified that THPE-NCs could transfer across KB cell membranes intact. As shown in Fig. 5, KB cell membranes were red after staining with DiI, a typical lipophilic membrane stain. Blue spots corresponding to THPE-NCs could be seen inside the red KB cell membranes inferring nanocrystal internalization into cells. Overall, stronger THPE fluorescence was observed at incubation with 24 μg/mL than that with 2.7 μg/mL. The results suggest that increased THPE-NC uptake was concentration-dependent and further imply that active transport may be involved in the absorption of THPE-NCs by KB cells. Note that the membrane staining was not uniform among the cells. The poor staining could result from unoptimized staining conditions including incubation time and chemical concentration. Additionally, several cells showed greater fluorescence intensities. This could be due to detrimental effects to the cell membrane by endocytosed nanocrystals, but remained to be further evaluated.

For both nanocrystals incubated respectively with 24 and 2.7 μg/mL, greater fluorescence was observed at 3 h compared to 1 h. However, no obvious difference was observed between 3 and 7 h. This indicates that cellular uptake of THPE-NCs may peak between 1 and 3 h, as well as the possibility that dissolution of the

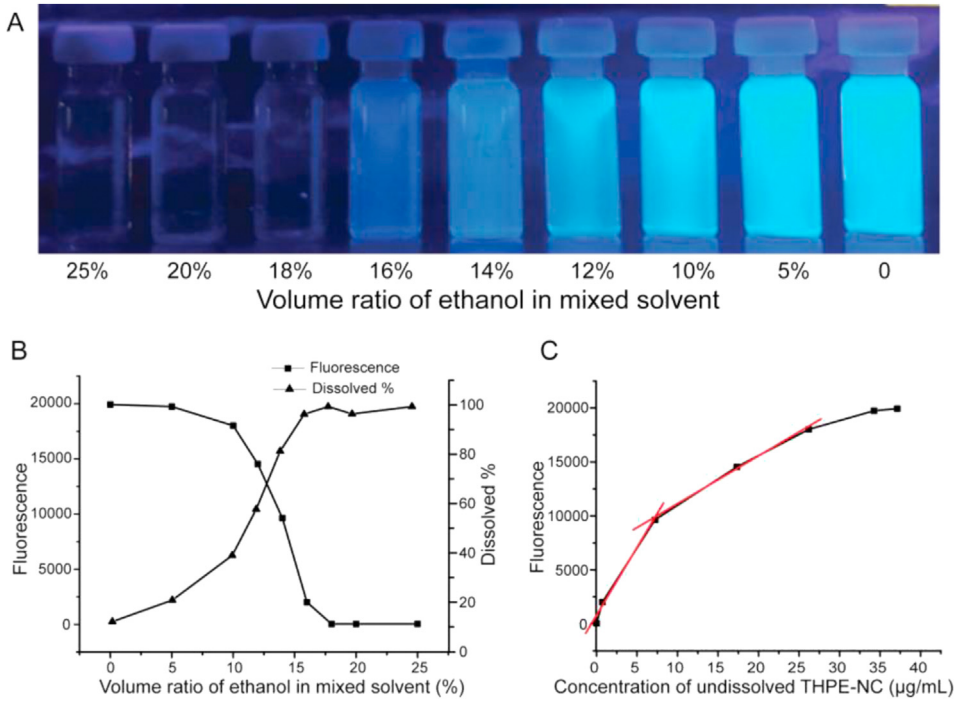

Figure 4 The AIE feature of THPE-NCs (A) Vials of THPE-NCs in water/ethanol mixtures of various *v*/*v* ratios under UV illumination (B) Fluorescence measured by fluorospectrometer and dissolved THPE measured by HPLC in the mixtures (C) The relationship between fluorescence and concentration of THPE-NCs.

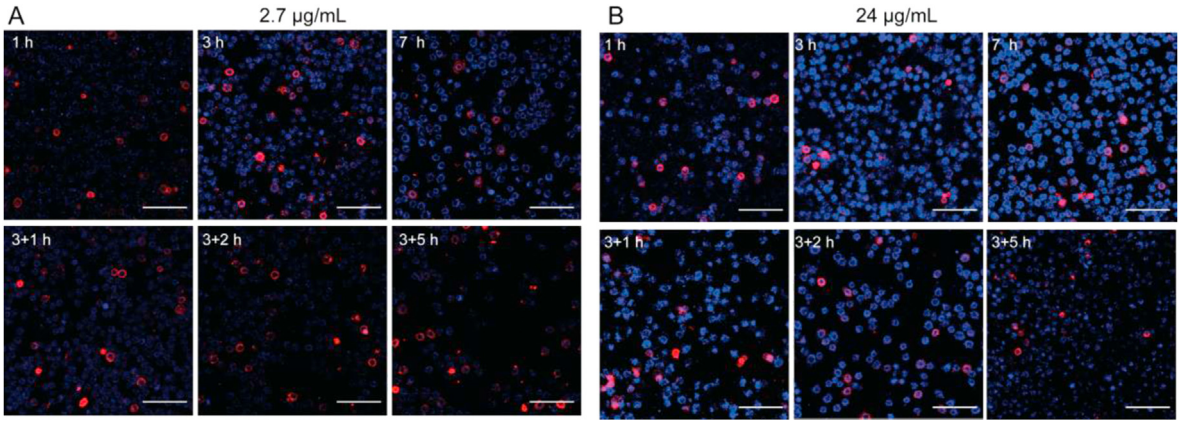

Figure 5 Confocal images of KB cells cultured with THPE-NCs at (A) 2.7 and (B) 24 μg/mL for 1, 3, 7 h, and additional 1, 2, and 5 h incubation with only fresh medium after 3 h of treatment. THPE was shown in blue and cell membrane in red. Scale bar = 100 μm.

nanocrystals and further cellular uptake of THPE-NCs approached a dynamically equilibrated state in terms of detected fluorescence intensity. An obvious decrease of THPE fluorescence appeared for an additional 1 h (2.7 μg/mL) and 5 h (24 μg/mL) after incubation with fresh media. This may be caused by dissolution and/or exocytosis of the intracellular THPE-NCs. It must also be noted that for 2.7 μg/mL, THPE-NC fluorescence continued to decrease up to an additional 2 h incubation with fresh media, with no significant reduction after 2 h. By contrast, THPE-NC fluorescence for 24 μg/mL group only decreased significantly after 5 h. This was likely because the concentration of intracellular THPE-NCs at 24 μg/mL was too high (up to 5 h) to sensitively detect fluorescence reduction due to nanocrystal dissolution and/or exocytosis by CLSM.

3.2.2. *Cellular uptake determined by flow cytometry*

Considering that confocal microscopy could not respond to subtle changes in fluorescence intensity, flow cytometry could offer higher sensitivity and was used to measure the intracellular fluorescence intensity (IFI) of single cells incubated with THPE-NCs. IFI determined for different treatments was shown in Fig. 6. According to the linear relationships established between fluorescence and concentration of THPE-NCs (Fig. 4), the relative IFI at different times compared with that of 0.5 h was calculated to indicate changes of intracellular THPE-NCs. The results are presented in Fig. 7 (the fitted lines in the figure are explained later). Note that the relative comparison should be interpreted semi-quantitatively, because the quantitative relationship (Fig. 4) was established in pure solution, not in an intracellular environment.

On the whole, flow cytometry determination reflected the same observations regarding drug uptake and removal as were seen with CLSM. Moreover, a distinct time and concentration dependence was observed. Significant changes in IFI were seen within the first 3 h of incubation for all three concentration groups ($P < 0.01$) as THPE-NC concentration increased. An increase in incubation time also improved IFI significantly ($P < 0.01$ or 0.05), except for 2.67 μg/mL group, at 3 h. This result corroborates with our previous study[31], in which uptake of PTX/TPE-NCs by KB cells showed a similar IFI time- and concentration-dependent trend. The higher the concentration of

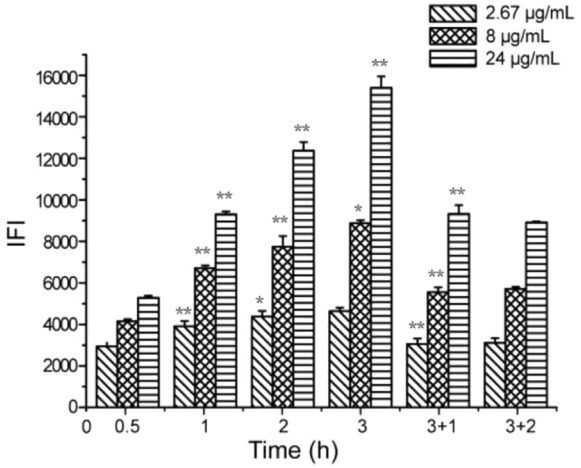

Figure 6 Intracellular fluorescence intensity (IFI) measured by flow cytometry after 0.5, 1, 2 and 3 h of incubation with THPE-NCs, respectively, as well as an additional 1 and 2 h incubation after removing NCs from the culture media at 3 h. Statistically significant difference between a data point and its previous time point of the same concentration is marked by $*P < 0.05$ or $**P<0.01$).

PTX/TPE-NCs, the larger the IFI became, comparably to what was observed in this study with THPE-NCs.

After THPE-NCs were removed from the culture media at 3 h, IFI greatly decreased at all three concentrations after an additional incubation time of 1 or 2 h, compared with IFI values at 3 h. Similar observation was also made with PTX/TPE-NCs[31]. This decline may be caused by THPE-NC dissolution in and/or efflux from cells. However, unlike PTX/TPE-NCs, no significant difference was detected between an additional incubation of 1 or 2 h ($P > 0.05$). There could be several possible reasons. For smaller concentrations (*i.e.*, 2.67 and 8 μg/mL), equilibrium between intra- and extracellular drug concentrations had likely been established after an additional hour of incubation. For higher concentrations (*i.e.*, 24 μg/mL), relative IFI only reduced from 2.85 to 2.66 between 1 and 2 additional hours of incubation. This may be due to the slow exocytosis and/or dissolution after one additional hour of incubation and the short time internal (1 h).

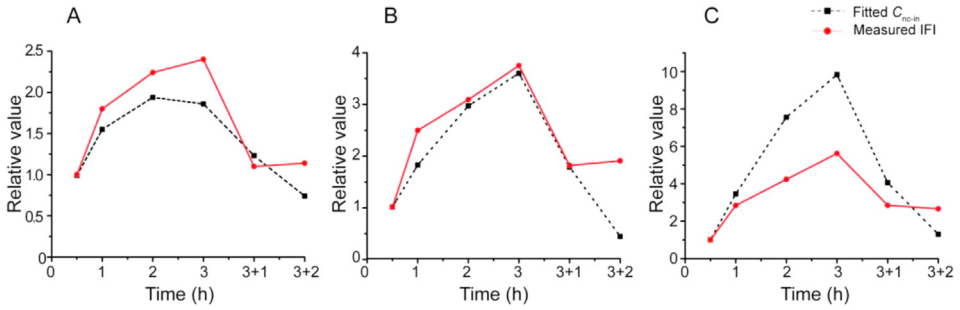

Figure 7 Relative intracellular concentration of THPE-NCs derived from IFI and PK modeling at 0.5, 1, 2 and 3 h of incubation with 2.67 (A), 8 (B), and 24 (C) μg/mL of THPE-NCs, respectively, as well as for an additional 1 and 2 h incubation after removing NCs from the culture media at 3 h. The value at 0.5 h is used as the reference.

3.2.3. *Cellular uptake determined by HPLC*

Dilution of THPE-NC suspensions to reach the desired concentrations (24, 8, and 2.6 μg/mL) resulted in changes in the total nanocrystal concentration due to dissolution equilibrium for each suspension. For samples with total THPE concentration of 2.67, 8 and 24 μg/mL, the undissolved THPE-NCs were 2.06 ± 0.02, 6.26 ± 0.08 and 20.23 ± 0.05 μg/mL, respectively.

The results shown in Fig. 8 indicated a steady rise of intracellular THPE within 3 h of incubation, confirming THPE uptake by KB cells. Extracellular THPE-NC dissolution appeared to reach an equilibrium within 2 h of incubation, after which THPE-NC concentration continued to decrease primarily through nanocrystal endocytosis. After 3 h, nanocrystals were removed and replaced with fresh media. At this point, intracellular THPE concentrations greatly declined after an additional incubation of 1 or 2 h, indicating exocytosis from cells. At the same time, both extracellular dissolved THPE and THPE-NC concentrations increased, although the dissolved THPE concentration was much higher than that of THPE-NC. Similar results were obtained for all three concentrations.

3.3. *PK modeling of cellular uptake kinetics*

Cellular uptake pharmacokinetics (PK) was modeled by Eqs. (1)−(4).

$$dC_{nc\_ex}/dt = -k_d(S - C_{mol\_ex}) + k_{nc\_ex}C_{nc\_in} - k_{nc\_en}C_{nc\_ex} \quad (1)$$

$$dC_{mol\_ex}/dt = k_d(S - C_{mol\_ex}) + k_{mol}(C_{mol\_in} - C_{mol\_ex}) \quad (2)$$

$$dC_{nc\_in}/dt = -k_d(S - C_{mol\_in}) + k_{nc\_en}C_{nc\_ex} - k_{nc\_ex}C_{nc\_in} \quad (3)$$

$$dC_{mol\_in}/dt = k_d(S - C_{mol\_in}) + k_{mol}(C_{mol\_ex} - C_{mol\_in}) \quad (4)$$

where S is the water solubility of THPE; C_{nc_ex}, C_{mol_ex}, C_{nc_in}, and C_{mol_in} are concentrations of extracellular nanocrystals, extracellular molecules, intracellular nanocrystals, and intracellular molecules, respectively. k_d is the dissolution rate constant of THPE nanocrystals, assumed to be the same in the extra- and intracellular space. k_{mol} is the transmembrane rate constant of THPE molecules, identical in both the endo- and exocytosis directions. It is assumed that molecular transmembrane movement is passive. k_{nc_ex} and k_{nc_en} are rate constants of nanocrystals in the exo- and endocytosis directions, respectively. The rate constants are different, based on the assumption that nanocrystal uptake and exocytosis are transporter-facilitated[35-37].

The ODE model was fitted against experimental HPLC data to determine the rate constant parameters (k_d, k_{mol}, k_{nc_ex} and k_{nc_en}). Because only the total amount of intracellular drug was determined, intracellular concentrations of dissolved THPE and THPE-NCs were also derived from the data fitting (Fig. 9). The fitted kinetics parameters were listed in Table 1. Using the derived rate parameters, respective concentration profiles were generated to mimic the incubation experiments when THPE-NCs were removed from extracellular culture media.

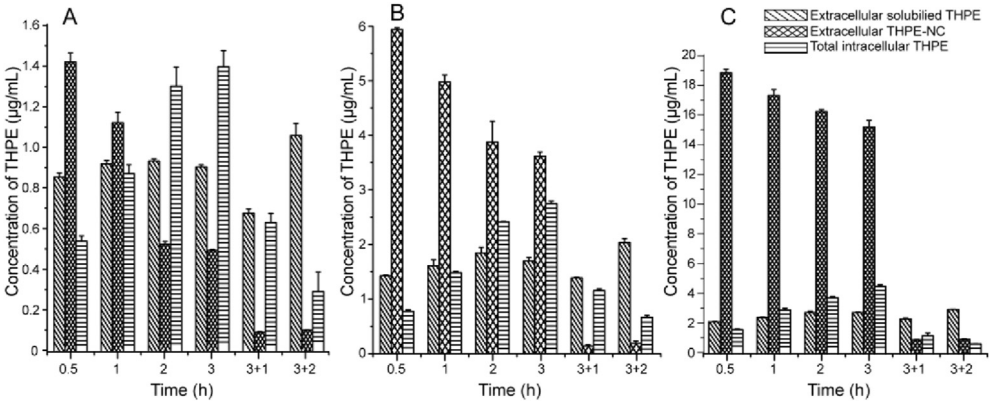

Figure 8 Cellular uptake measurement of KB cells by HPLC after 0.5, 1, 2 and 3 h of incubation with 2.67 (A), 8 (B), and 24 (C) μg/mL of THPE-NCs, respectively, as well as an additional 1 and 2 h incubation after removing NCs from the culture media at 3 h.

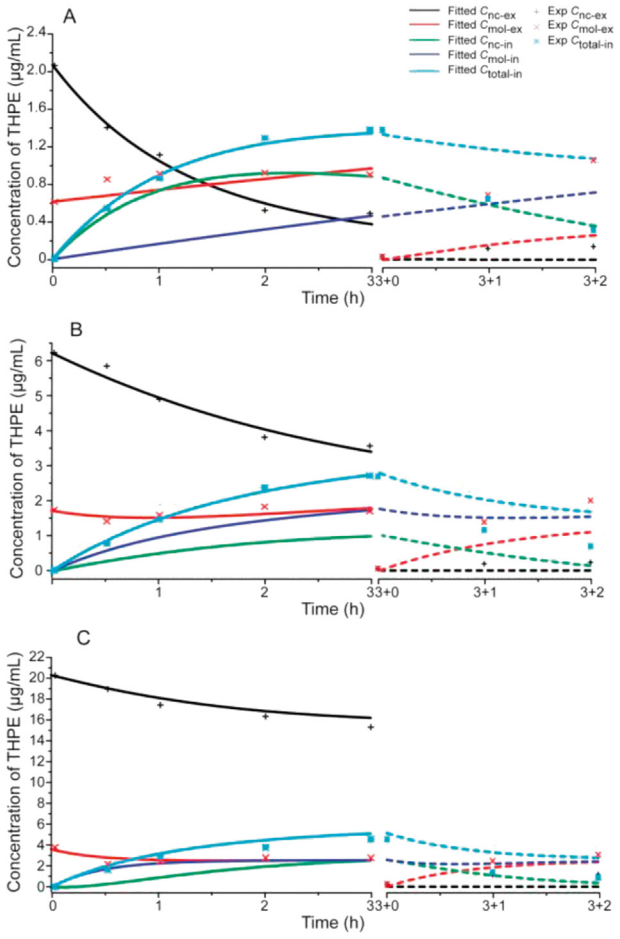

Figure 9 The fitted (line) and predicted curves (dash line) of cellular uptake in KB cells after 0.5, 1, 2 and 3 h incubation with 2.67 (A), 8 (B), and 24 (C) μg/mL of THPE-NCs, respectively, as well as an additional 1 and 2 h incubation after removing the drug from the culture media at 3 h. Experimentally measured data are shown as dot.

Table 1 Simulation-derived kinetics parameters.

Parameter	2.67 μg/mL	8 μg/mL	24 μg/mL
k_d	0.065	0.250	1.200
k_{nc_en}	0.667	0.200	0.123
k_{nc_ex}	0.225	0.347	0.614
k_{mol}	0	0.434	0.710
Sum of squared residues	0.1022	0.2737	3.638

Fitting of the PK model to the experimental data appeared to be tight, given the small sum of squared reside values between the fitted and experimental data. As shown in Table 1, THPE-NC concentrations of 2.67 and 8 μg/mL had relatively better fitting quality than 24 μg/mL, with sum of squares of residuals being 0.1022 and 0.2737, respectively. Table 1 also showed that the simulated kinetics parameters were dependent on the suspension concentration of THPE-NCs. As concentration increased, dissolution (k_d) and exocytosis ($k_{nc\text{-}ex}$) of the nanocrystals, and cross-membrane diffusion of the molecules (k_{mol}) increased, but nanocrystal endocytosis ($k_{nc\text{-}en}$) decreased. For 2.67 μg/mL only, endocytosis was faster than exocytosis. A k_{mol} of zero was determined for this concentration, from the data fitting. This was likely caused by the fact that only 22.8% of THPE existed as dissolved molecules in the THPE-NC suspension, with the lowest dissolved concentration of 0.61 μg/mL. At the same time, a k_d of 0.065 meant that very little intracellular THPE-NC dissolution occurred. Thus, a very small concentration gradient existed for dissolved THPE to move across the cell membrane, resulting in the negligible k_{mol} value.

The poorer fitting parameters for 24 μg/mL may be due to several reasons. One was that the significantly high THPE-NC concentration, compared to 2.67 and 8 μg/mL, mathematically put more weight on the fitting resulting in the larger sum of squared residues (Table 1). Another was that true equilibrium may not have been established within the time of incubation, given that the extracellular dissolved THPE concentration was 3.6 μg/mL (significantly higher than the aqueous solubility of 2.6 μg/mL).

Intracellular THPE-NC concentrations could not be determined accurately by HPLC, as separation methods such as ultracentrifugation would destroy the equilibrium between intact and dissolved nanocrystals. On the other hand, flow cytometry was capable of measuring the fluorescence of THPE-NCs in KB cells, thereby indirectly measuring intracellular THPE-NC concentrations. The measured IFI and calculated $C_{nc\text{-}en}$ at different time-points, normalized against the values at 0.5 h, were therefore compared. Fig. 7 showed that for 2.67 or 8 μg/mL, a good fit was achieved, suggesting that the change of calculated $C_{nc\text{-}en}$ seemed to corroborate with the relative IFI at 1, 2 and 3 h. Subsequently, after the additional incubation with fresh media, a consistent trend between the percent change in measured and calculated $C_{mol\text{-}ex}$ was also seen, despite the difference in absolute values of concentration used. Calculated $C_{mol\text{-}ex}$ increased by 62.5% and 44.7% for the 2.67 and 8 μg/mL groups, respectively, and the measured $C_{mol\text{-}ex}$ increased by 56.7% and 46.7%, respectively. This suggested that the fitting model was successful in estimating intracellular THPE-NC values.

However, the fitted ODE model deviated from experimental data after incubation of cells with fresh media. One ostensible reason lies in inherent limitations of the PK model, in which several assumptions were made. First, cross-membrane transport of dissolved THPE was regarded as passive. However, it was unclear whether, and to what extent, transporter-assisted or receptor-mediated pathways existed for THPE. Second, dissolution kinetics was treated identical for both intra- and extracellular nanocrystals. The rationale behind this assumption lies in THPE's very low solubility and being a non-electrolyte. While its solubility is different between the intra and extracellular space because of the variation in environmental makeups, such difference could be marginal as compared with experimental errors in measurement. Nonetheless, it is possible that nanocrystals dissolved slower inside cells because of the differences in intracellular liquid volume and composition. Further investigation was thus warranted. Third, k_{nc_en} *vs.* k_{nc_ex} would likely change in situations where no extracellular THPE was present, leading to model discrepancies when using the same rate parameter values before and after removal of extracellular THPE. Finally, measurement uncertainties, such as those involved in separating nanocrystals from cellular components using centrifugation, also existed. Regardless, the simulated results indicated that, when extracellular THPE-NCs were removed, equilibrium shifted to complete dissolution of all

intracellular NCs, followed by passive molecular exocytosis. Both experimental and simulation results hinted that it was easier for a nanocrystal to be taken up by a cell than to be released. These mechanisms may be different, and/or require different energy input, and would be investigated in future studies.

4. Conclusions

This study used THPE, an AIE fluorophore, as a model compound to explore cellular uptake mechanisms and dissolution kinetics of nanocrystals inside cells. Confocal imaging and flow cytometry indicated that nanocrystals could be taken up directly by cells in the form of solid nanoparticles as well as dissolved molecules. Flow cytometry and HPLC analysis suggested that cellular uptake kinetics of NCs were concentration-dependent. Compared with our previous study of PTX/TPE-NCs[31], similar changes in intracellular fluorescence distribution and intensity, as well as intra or extracellular drug content were observed during incubation with nanocrystals and additional incubation with fresh media. Kinetic simulation further indicated that exocytosis of intracellular THPE-NCs bore different kinetics and/or mechanisms compared with endocytosis, possibly due to limited intracellular dissolution and a greater energy requirement to transport NCs to the environment.

The observation made with a dye molecule in this study alludes that nanocrystals of a pharmaceutical compound can be internalized by cells and the endocytosed nanocrystals dissolve and release drug molecules that further diffuse out of the cells. Moreover, because solubility and other particulate properties (including particle size and crystal morphology) vary significantly from one compound to another, it is expected that for nanocrystals of a different chemical, its cellular update kinetics may be drastically distinct.

Acknowledgements

Jinfeng Zhang acknowledged the financial support by the China Scholarship Council (No.201806995008, China) and Key Projects of Chinese Medicine Research of Chongqing Municipal Health Bureau (ZY201701004, China). Clairissa D. Corpstein and Tonglei Li thanked the Chao Endowment and Purdue Research Foundation for support (USA).

Author contributions

Jifen Zhang and Tonglei Li designed the research. Jifen Zhang carried out the experiments. Jifen Zhang and Tonglei Li performed data analysis. Clairissa D. Corpstein participated part of the experiments. Tonglei Li provided experimental drugs and quality control. Jifen Zhang wrote the manuscript. Tonglei Li and Clairissa D. Corpstein revised the manuscript. All of the authors have read and approved the final manuscript.

Conflicts of interest

The authors have no conflicts of interest to declare.

References

1. Peltonen L, Hirvonen J. Drug nanocrystals—versatile option for formulation of poorly soluble materials. *Int J Pharm* 2018;**537**:73–83.
2. Jassim ZE, Rajab NA. Review on preparation, characterization, and pharmaceutical application of nanosuspension as an approach of solubility and dissolution enhancement. *J Pharm Res* 2018;**12**:771–4.
3. Jermain SV, Brough C, Williams RO. Amorphous solid dispersions and nanocrystal technologies for poorly water-soluble drug delivery—an update. *Int J Pharm* 2018;**535**:379–92.
4. Raghava Srivalli KM, Mishra B. Drug nanocrystals: a way toward scale-up. *Saudi Pharmaceut J* 2016;**24**:386–404.
5. Gao L, Zhang DR, Chen MH. Drug nanocrystals for the formulation of poorly soluble drugs and its application as a potential drug delivery system. *J Nano Res* 2008;**10**:845–62.
6. Chen A, Shi Y, Yan ZQ, Hao HX, Zhang Y, Zhong J, et al. Dosage form developments of nanosuspension drug delivery system for oral administration route. *Curr Pharml Design* 2015;**21**:4355–65.
7. Malamatari M, Taylor KMG, Malamataris S, Douroumis D, Kachrimanis K. Pharmaceutical nanocrystals: production by wet milling and applications. *Drug Discov* 2018;**23**:534–47.
8. Ahire E, Thakkar S, Darshanwad M, Misra M. Parenteral nanosuspensions: a brief review from solubility enhancement to more novel and specific applications. *Acta Pharm Sin B* 2018;**8**:733–55.
9. Chen ZJ, Wu W, Lu Y. What is the future for nanocrystal-based drug-delivery systems?. *Ther Deliv* 2020;**11**:225–9.
10. Jarvis M, Krishnan V, Mitragotri S. Nanocrystals: a perspective on translational research and clinical studies. *Bioeng Transl Med* 2019;**4**:5–16.
11. Mohammad IS, Hu HY, Yin LF, He W. Drug nanocrystals: fabrication methods and promising therapeutic applications. *Int J Pharm* 2019;**562**:187–202.
12. Maria G, Cristina C, Roberta C, Gigliobianco MR, Casadidio C, Censi R, et al. Nanocrystals of poorly soluble drugs: drug bioavailability and physicochemical stability. *Pharmaceutics* 2018;**10**:134–62.
13. Areen A, Gábor K, Ildikó C, Ambrus R. Design and characterization of loratadine nanosuspension prepared by ultrasonic-assisted precipitation. *Eur J Pharmaceut Sci* 2018;**122**:90–104.
14. Singh MK, Pooja D, Ravuri HG, Gunukula A, Kulhari H, Sistla R. Fabrication of surfactant-stabilized nanosuspension of naringenin to surpass its poor physiochemical properties and low oral bioavailability. *Phytomedicine* 2018;**40**:48–54.
15. Omolo CA, Kalhapure RS, Agrawal N, Rambharose S, Mocktar C, Govender T. Formulation and molecular dynamics simulations of a fusidic acid nanosuspension for simultaneously enhancing solubility and antibacterial activity. *Mol Pharm* 2018;**15**:3512–26.
16. Shah DA, Murdande SB, Dave RH. A review: pharmaceutical and pharmacokinetic aspect of nanocrystalline suspensions. *J Pharm Sci* 2016;**105**:10–24.
17. Lu Y, Qi JP, Dong XC, Zhao WL, Wu W. The *in vivo* fate of nanocrystals. *Drug Discov Today* 2017;**22**:744–50.
18. Hu XW, Dong XC, Lu Y, Qi JP, Zhao WL, Wu W. Bioimaging of nanoparticles: the crucial role of discriminating nanoparticles from free probes. *Drug Discov Today* 2017;**22**:382–7.
19. Fu Q, Sun J, Ai XY, Zhang P, Li M, Wang YJ, et al. Nimodipine nanocrystals for oral bioavailability improvement: role of mesenteric lymph transport in the oral absorption. *Int J Pharm* 2013;**448**:290–7.
20. Miao XQ, Li Y, Wang XQ, Yuen Lee SM. Transport mechanism of coumarin 6 nanocrystals with two particle sizes in MDCKII monolayer and larval zebrafish. *ACS Appl Mater Interfaces* 2016;**8**:12620–30.
21. Vidlářová L, Romero GB, Hanuš J, Štěpánek F, Müller RH. Nanocrystals for dermal penetration enhancement—effect of concentration and underlying mechanisms using curcumin as model. *Eur J Pharm Biopharm* 2016;**104**:216–25.
22. Hollis CP, Weiss HL, Leggas M, Evers BM, Gemeinhart RA, Li TL. Biodistribution and bioimaging studies of hybrid paclitaxel nanocrystals: lessons learned of the EPR effect and image-guided drug delivery. *J Control Release* 2013;**172**:12–21.
23. Hollis CP, Weiss HL, Evers BM, Gemeinhart RA, Li TL. *In vivo* investigation of hybrid paclitaxel nanocrystals with dual fluorescent probes for cancer theranostics. *Pharm Res (N Y)* 2014;**31**:1450–9.

24. He Y, Xia DN, Li QX, Tao JS, Gan Y, Wang C. Enhancement of cellular uptake, transport and oral absorption of protease inhibitor saquinavir by nanocrystal formulation. *Acta Pharmacol Sin* 2015;**36**:1151−60.
25. Xie YK, Shi BK, Xia F, Qi JP, Dong XC, Zhao WL, et al. Epithelia transmembrane transport of orally administered ultrafine drug particles evidenced by environment sensitive fluorophores in cellular and animal studies. *J Control Release* 2018;**270**:65−75.
26. Liu DL, Wan B, Qi JP, Dong XC, Zhao WL, Wu W, et al. Permeation into but not across the cornea: bioimaging of intact nanoemulsions and nanosuspensions using aggregation-caused quenching probes. *Chin Chem Lett* 2018;**29**:1834−8.
27. Zheng SC, Huang CH, Zhao XY, Zhang Y, Liu SW, Zhu QH. A hydrophobic organelle probe based on aggregation-induced emission: nanosuspension preparation and direct use for endoplasmic reticulum imaging in living cells. *Spectrochim Acta* 2018;**189**:231−8.
28. Donnier-Maréchal M, Abdullayev S, Bauduin M, Pascal Y, Fu MQ, He XP, et al. Tetraphenylethylene-based glycoclusters with aggregation-induced emission (AIE) properties as high-affinity ligands of bacterial lectins. *Org Biomol Chem* 2018;**16**:8804−9.
29. Bian N, Chen Q, Qiu XL, Qi AD, Han BH. Imidazole-bearing tetraphenylethylene: fluorescent probe for metal ions based on AIE feature. *New J Chem* 2011;**35**:1667−71.
30. Chen Y, Li TL. Cellular uptake mechanism of paclitaxel nanocrystals determined by confocal imaging and kinetic measurement. *AAPS J* 2015;**17**:1126−34.
31. Gao W, Lee D, Meng ZJ, Li TL. Exploring intracellular fate of drug nanocrystals with crystal-integrated and environment-sensitive fluorophores. *J Control Release* 2017;**267**:214−22.
32. Xue XD, Zhao YY, Dai LR, Zhang X, Hao XH, Zhang CQ, et al. Spatiotemporal drug release visualized through a drug delivery system with tunable aggregation-induced emission. *Adv Mater* 2014;**26**:712−7.
33. Wang X, Yang YY, Yang F, Shen H, Wu DC. pH-triggered decomposition of polymeric fluorescent vesicles to induce growth of tetraphenylethylene nanoparticles for long-term live cell imaging. *Polymer* 2017;**118**:75−84.
34. Gu XG, Yao JQ, Zhang GX, Zhang C, Yan YQ, Zhao YS, et al. New electron-donor/acceptor-substituted tetraphenylethylene: aggregation-induced emission with tunable emission color and optical-waveguide behavior. *Chem Asian J* 2013;**8**:2362−9.
35. Tu LX, Cheng M, Sun YB, Fang YY, Liu JL, Liu W, et al. Fabrication of ultra-small nanocrystals by formation of hydrogen bonds: *in vitro* and *in vivo* evaluation. *Int J Pharm* 2020;**573**:118730.
36. Sheng HG, Zhang YN, Nai JJ, Wang SH, Dai MM, Lin GT, et al. Preparation of oridonin nanocrystals and study of their endocytosis and transcytosis behaviours on MDCK polarized epithelial cells. *Pharm Biol* 2020;**58**:518−27.
37. Guo MR, Wei MD, Li W, Guo MC, Guo CL, Ma MC, et al. Impacts of particle shapes on the oral delivery of drug nanocrystals: mucus permeation, transepithelial transport and bioavailability. *J Control Release* 2019;**307**:64−75.